

Analysis of a carbon dimer bound to a vacancy in iron using density functional theory and a new tight binding model

A. T. Paxton^{1,2,*} and C. Elsässer^{1,3,†}

¹*Fraunhofer Institut für Werkstoffmechanik IWM,
Wöhlerstr. 11, 79108 Freiburg, Germany*

²*Atomistic Simulation Centre, School of Mathematics and Physics,
Queen's University Belfast, Belfast BT7 1NN, UK*

³*Karlsruher Institut für Technologie,
Institut für Ausgewandte Materialien (IAM-ZBS),
Kaiserstr. 12, 76131 Karlsruhe, Germany*

(Dated: October 31, 2018)

Abstract

Recent density functional theory (DFT) calculations by Först *et al.*¹ have predicted that vacancies in both low and high carbon steels have a carbon dimer bound to them. This is likely to change the thinking of metallurgists in the kinetics of the development of microstructures. While the notion of a C₂ molecule bound to a vacancy in Fe will potentially assume a central importance in the atomistic modeling of steels, neither a recent tight binding (TB) model nor existing classical interatomic potentials can account for it. Here we present a new TB model for C in Fe, based on our earlier work for H in Fe, which correctly predicts the structure and energetics of the C₂ dimer at a vacancy in Fe. Moreover the model is capable of dealing with both concentrated and dilute limits of carbon in both α -Fe and γ -Fe as comparisons with DFT show. We use both DFT and TB to make a detailed analysis of the dimer and to come to an understanding as to what governs the choice of its curious orientation within the vacancy.

PACS numbers: 71.20.Be 75.50.Bb 73.20.Hb 68.43.Fg

I. INTRODUCTION

A great deal of progress over many years has been made in understanding the *physics* of the bonding and electronic structure in pure magnetic iron² and this has been used with great effect to advance the generation of schemes from density functional theory in the gradient corrected³ local spin density approximation^{4,5} (LSDA-GGA) through the tight binding approximation^{6,7} to classical interatomic potentials to be used for atomistic simulations by the *materials science* community.⁸ Of course the metallurgist is rarely interested in pure iron and so the challenge to the physicist has been to extend the theory to include interstitial carbon, which is the defining element whose presence distinguishes steel from iron. It is only in the last decade that real progress has been made; first with some very extensive LSDA-GGA calculations,^{1,9-13} second with the generation of (admittedly very complicated) classical interatomic potentials based in the embedded atom method,^{11,14} and third, the subject of this paper, by some recent semi empirical quantum mechanical schemes based in the tight binding approximation. A particularly significant advance was made recently by Hatcher, Madsen and Drautz¹⁵ who constructed a very simple orthogonal tight binding model for carbon and iron using a minimal basis of C-*p* and Fe-*d* orbitals and a local charge neutrality condition. This model is a natural basis for a bond order potential,¹⁶ but we argue here that this basis may be too small to capture some of the physics of carbon in iron. Instead we introduce a new model based in our earlier work on H in Fe¹⁷ employing a larger, non orthogonal basis of C-*p*, Fe-*d*, and C and Fe-*s* orbitals and treating charge transfer self consistently *via* an adjustable “Hubbard-*U*” parameter.¹⁸ The structure of the paper is as follows. In section II we describe our new model for carbon in iron and in section III we demonstrate its predictive power in both the concentrated (iron carbide) and dilute impurity limits. In III C we focus on the carbon dimer bound to a vacancy, taking in view the recent startling prediction from LSDA-GGA that this is a predominant point defect in steel.¹ Our discussion and conclusions are to be found in sections IV and V.

II. DESCRIPTION OF THE NEW MODEL

We take the same approach as in our earlier work on H in Fe¹⁷ which is similar to that of Hatcher *et al.*¹⁵ on C in Fe, namely to proceed from a given model for pure Fe and generate a

further parameterization for the interstitial element. In contrast to Hatcher *et al.*¹⁵ we do not use a direct projection of the LSDA-GGA Hamiltonian onto a tight binding basis,^{19,20} instead we employ a genetic algorithm²¹ to fit the parameters to a small set of LSDA-GGA target data which enter an objective function, which is minimized. As a consequence of employing the simplest tight binding scheme, namely an orthogonal basis of only *d*-orbitals on the Fe atoms and *p*-orbitals on the C atoms, the model of Hatcher *et al.*¹⁵ differs significantly from ours. One difference results from their underlying model for pure Fe which includes an *attractive* bonding term in the total energy which is environment dependent and which accounts for a significant fraction of the total energy.¹⁹ This was intended as a surrogate for the missing *s*-electrons, but the fact that this term is large and *negative* is surprising as one expects the *s*-band to exert a *positive* pressure.^{22–24} Another difference is that in the minimal basis having only *p*-orbitals on C atoms the limit of pure carbon can only be approximately rendered since it is the *sp*-hybridisation in carbon that leads to the rich variety of single, double and triple bonds and the competition between *sp*²-bonded graphite and *sp*³-bonded diamond. We will argue below that carbon *sp*-hybridization plays a key role in the structural stability of iron carbides and also in controlling the configuration of the C₂ dimer at an Fe vacancy. Therefore in the current work we employ a larger basis, namely *s*- and *d*-orbitals on Fe and *s*- and *p*-orbitals on C atoms from which we suppose that at the expense of greater computational cost we have a physically better motivated model. Moreover we use a *non orthogonal* basis, and as we argued earlier¹⁷ we believe that this allows a more natural way to include environment dependence in the bond energy.

The tight binding model that we present here is identical in its mathematical form to those we developed earlier.¹⁷ The functional forms of the bond and overlap integrals are

$$h(r) = h_0 e^{-qr} \quad s(r) = s_0 e^{-qr}$$

and we tabulate all parameter values h_0 and s_0 in tables I (for Fe–Fe terms) and V (for Fe–C interactions). The Fe–Fe and Fe–C pair potentials are

$$\phi(r) = B_1 e^{-p_1 r} - B_2 e^{-p_2 r}$$

noting the sign, so that in tables I and V parameter values for B_1 and B_2 are positive. For Fe–H the pair potential is

$$\phi(r) = \frac{B_1}{r} e^{-p_1 r}$$

TABLE I. Intersite bond integral and pair potential parameters for the Fe–Fe terms in our tight binding model. All quantities are in Rydberg atomic units (a.u.) except for the cut off radii, r_1 and r_c which are in units of the equilibrium bcc lattice constant $a_0^{\text{bcc}}=2.87\text{\AA}$. We include models using both volume-scaled and fixed cut offs (see the text). These differ only in their pair potentials and are indicated as “sc” and “fx” respectively in the last four rows. Properties of pure Fe resulting from these four models are displayed in table II. Parameters for C and H in Fe in table V and used in the remainder of this paper are associated with the fixed cut off sd -model (sd -fx). We note that these parameters differ from those published earlier;¹⁷ first by correcting misprints in the decay constant q in the $ss\sigma$ and $sd\sigma$ terms, second because we have moved the cut off r_1 from 10% larger to 10% smaller than a_0^{bcc} . Third we now prefer fixed multiplicative to scaled augmentative cut offs. See also the text. These differences are then reflected in slightly different calculated properties in table II.

$ss\sigma$		$sd\sigma$		$dd\sigma$	$dd\pi$	$dd\delta$
h_0	s_0	h_0	s_0	h_0	h_0	h_0
-0.35	0.45	-0.14067	0.5	-2.4383	1.9972	-0.90724
————— $q = 0.3$ —————				————— $q = 0.9$ —————		
————— $r_1 = 1.1$ —————				————— $r_1 = 0.9$ —————		
————— $r_c = 2.0$ —————				————— $r_c = 1.4$ —————		
B_1		p_1	B_2	p_2	r_1	r_c
sd -fx	698.67	1.52	517.467	1.4576	0.9	1.4
sd -sc	665.60	1.40843	536.800	1.36297	0.9	1.4
d -fx	683.1	1.5376	459.5	1.4544	0.9	1.4
d -sc	682.8	1.5165	466.8	1.4350	0.9	1.4

TABLE II. Properties of pure α -Fe. Target elastic constants are taken from experimental low temperature data (see ref [17]); theoretical hcp–bcc energy difference from our own LSDA-GGA calculations; experimental vacancy formation and migration energies are from Seeger,²⁵ while remaining LSDA-GGA data are from Domain and Bequart,⁹ and Kabir *et al.*¹³ We show four models in data columns 1–4: canonical (*d*) with scaled (*sc*) and fixed (*fx*) cut offs and non orthogonal (*sd*) with scaled and fixed cut offs respectively.

	<i>d-sc</i>	<i>d-fx</i>	<i>sd-sc</i>	<i>sd-fx</i>	target	
K (Gpa)	161	174	185	192	168	(expt.)
C' (GPa)	50	50	55	45	53	(expt.)
c_{44} (Gpa)	118	117	106	100	122	(expt.)
$\Delta E_{\text{hcp-bcc}}$ (mRy)	8	6	6	6	15	(LSDA-GGA)
$H_{\text{Vac}}^{\text{F}}$ (eV)	2.0		1.6		1.61–1.75	(expt.)
					2.0	(LSDA-GGA)
$H_{\text{Vac}}^{\text{M}}$ (eV)	1.16		0.81		1.12–1.34	(expt.)
					0.65–0.75	(LSDA-GGA)

We take a rather sophisticated approach to cutting off the spacial dependence of these interactions. We require proper energy conservation in molecular dynamics and cannot allow discontinuities in second derivatives of bond integral or pair potential functions. Previously¹⁷ we implemented the cut off by *augmenting* (that is, replacing) the function with a polynomial of degree five within $r_1 < r < r_c$ whose coefficients are chosen so as to match the function continuously and differentially to its *value* at r_1 and to *zero* at r_c . We chose $r_1 = 1.1a_0^{\text{bcc}}$ and $r_c = 1.4a_0^{\text{bcc}}$, where $a_0^{\text{bcc}} = 2.87 \text{ \AA}$ is the lattice constant of α -Fe, so that functions are cut off to zero between second and third neighbors of the bcc lattice. Subsequent improvements were introduced after making two observations.²⁶ (*i*) A smoother effect can be achieved using a *multiplicative* cut off; that is, to multiply the function by a polynomial of degree five whose value is one at r_1 and zero at r_c and whose coefficients again ensure that the function is everywhere continuous up to the second derivative. (*ii*) Because the multiplicative cut off “inherits” the shape of the function near r_1 better than the augmentative cut off, we found that we could move r_1 back to $0.9a_0^{\text{bcc}}$ and achieve a smoother function overall. A second difference compared to our earlier work¹⁷ is that there we employed a volume dependent cutoff, whereas now we prefer to use a cut off that is fixed. Because of this

TABLE III. On-site Hamiltonian matrix elements for tight binding models of Fe, H and C. U is the Hubbard- U parameter and J is the Stoner parameter.^{5,7} All quantities are in Rydberg atomic units (a.u.); N_d is the number of d -electrons, which is an adjustable parameter in the canonical model.

	$\varepsilon_s - \varepsilon_d^{\text{Fe}}$	$\varepsilon_p - \varepsilon_d^{\text{Fe}}$	N_d	U	J
Fe- d			7		0.05
Fe- sd	0.15			1.0	0.055
C	-0.468	0.083		1.238	0
H	-0.085			1.2	0

small modification it is necessary to obtain slightly amended pair potential parameters. We show these in table I, and in table II some predicted properties of pure Fe using both the canonical d -band model for Fe and the non orthogonal sd -model. Our canonical model can be read from table I simply by ignoring those parameters that don't enter the Hamiltonian. This model therefore differs from the canonical model that we published earlier.¹⁷ In fact it is worth pointing out that both these canonical d -band models reproduce the vacancy formation and migration energies better than our non orthogonal model; although its $H_{\text{Vac}}^{\text{F}}$ is outside the experimental range it is in better agreement with published LSDA-GGA data. In our opinion the simplest canonical model is very appropriate for pure Fe and we do not see the need for the additional, attractive “embedding potential” introduced by Madsen *et al.*¹⁹ The inclusion of the s -band and non orthogonality in Fe is only necessary once hydrogen or first row elements are included. The reason for this is that the valence s -band from these elements lies typically below the Fe $3d$ -bands; orthogonality constraints in the concentrated limit then push the Fe $4s$ -band to above the Fermi level. In the dilute limit the electronic structure has to differentiate between regions close to an impurity and those far from it where the iron $4s$ local density of states returns to its position in pure Fe below the Fermi level. To account properly for this effect the impurity and Fe s -bands cannot be neglected. Of course in a minimal pd basis for Fe-C tight binding models or bond order potentials *both* s -bands are neglected which is internally consistent, but these models cannot account for, say, the carbon sp -hybridisation.

FIG. 1. (color online) Structural energy–volume curves for the four iron monocarbide phases, FeC, that were used in the fitting of the tight binding model. These show the heat of formation as a function of the atomic volume per Fe atom in both bcc (α) and fcc (γ) Fe each containing C atoms in tetrahedral (TET) or octahedral (OCT) interstices. Note that the atomic volume, Ω_0 , of pure α -Fe is 79.765 a.u. In this, and subsequent figures, GGA denotes the generalized gradient approximation to the LSDA.

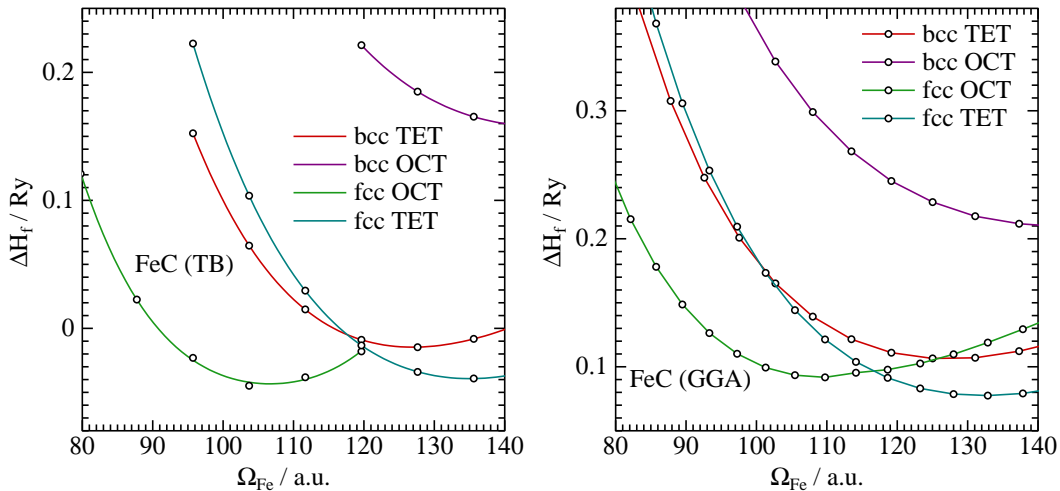


TABLE IV. Properties of iron monocarbides. These are the atomic volume of Fe, Ω_{Fe} , in FeC relative to $\Omega_0 = (a_0^{\text{bcc}})^3/2$ in the four monocarbides obtained from bcc α -Fe and fcc γ -Fe in which C is in either tetrahedral or octahedral interstices. ΔE is the energy difference per formula unit in Ry compared to the fcc octahedral compound. Targets are taken from our LSDA-GGA calculations.

	α -tet		α -oct		γ -tet		γ -oct
	$\Omega_{\text{Fe}}/\Omega_0$	ΔE	$\Omega_{\text{Fe}}/\Omega_0$	ΔE	$\Omega_{\text{Fe}}/\Omega_0$	ΔE	$\Omega_{\text{Fe}}/\Omega_0$
TB	1.591	0.030	1.832	0.202	1.690	0.005	1.327
target	1.549	0.020	1.788	0.147	1.613	-0.010	1.339

A. The on-site carbon and Fe–C parameters

Our approach to finding carbon on-site energy parameters, Fe–C Hamiltonian matrix elements and pair potential parameters is to fit these to just seven target data (a refinement was done later to improve the model in the dilute limit, see section III B). These data are taken from LSDA-GGA calculations and illustrated in figure 1 which shows the heat of formation of four compounds having the stoichiometry FeC. These are either bcc α -Fe or fcc γ -Fe with C interstitials in tetrahedral or octahedral sites. In the γ -Fe case these are identical to the zincblende and rocksalt crystal structures. We fitted our parameters to the four equilibrium volumes and three energy differences. The outcomes of the fitting are shown to the left of figure 1 and in table IV. The resulting parameter values are tabulated in tables I, III, and V. For comparison and for completeness we also show parameters of our earlier model for hydrogen in Fe.¹⁷

It is important to make some comments about the energy–volume curves in figure 1, also in relation to the equivalent data for the hydrogen interstitial.¹⁷ First, in the bcc structure both C and H prefer the tetrahedral site in the concentrated limit of FeC and FeH, and this remains the preferred site for H into the dilute limit. In contrast carbon occupies the octahedral sites in both ferritic and austenitic steel. In α -Fe, this is achieved at the expense of a local tetragonal distortion of the lattice so as to drive apart the two apical Fe atoms in the irregular octahedron of the underlying bcc lattice. This is only possible if the C is sufficiently dilute, certainly more dilute than the stoichiometry Fe₄C, as we will see below, and in fact the crossover is around Fe₁₆C.²⁷ Second, in the fcc structure it is certainly striking that according to LSDA-GGA FeC adopts the zincblende structure rather than the rocksalt structure, albeit at an expanded volume, as the tetrahedral interstice is much smaller than the octahedral. This is contrary to the behavior of hydrogen, even though its atomic radius is evidently smaller. Again there is a crossover towards the dilute limit where C prefers the octahedral site in γ -Fe.²⁷ We expect that the competition between the two sites in FeC is driven by the *sp*-hybridization which will be maximal in the four fold coordinated tetrahedral site, whereas the six fold octahedral site offers a bonding environment favorable to the 90° bond angles of unhybridised *p*-orbitals. Therefore it is surprising that the *pd*-basis model¹⁵ reproduces this result correctly. We expect that this arises from the freedom of employing long ranged C–C interactions in that model.¹⁵ Conversely we take the canonical point of view

TABLE V. Intersite bond integrals and pair potential parameters for the Fe–C and Fe–H terms. All quantities are in Rydberg atomic units (a.u.) except for the cut off radii, r_1 and r_c which are in units of the equilibrium bcc lattice constant $a_0^{\text{bcc}} = 2.87\text{\AA}$. This corrects two misprints regarding the $ss\sigma$ and $sd\sigma$ bond integrals for Fe–H in table V of ref [17].

	$ss\sigma$		$sp\sigma$		$sd\sigma$		$pd\sigma$		$pd\pi$	
	h_0	s_0	h_0	s_0	h_0	s_0	h_0	s_0	h_0	s_0
	q	q	q	q	q	q	q	q	q	q
	r_1	r_1	r_1	r_1	r_1	r_1	r_1	r_1	r_1	r_1
	r_c	r_c	r_c	r_c	r_c	r_c	r_c	r_c	r_c	r_c
Fe–C	-1.7712	0.38434	3.9546	-0.59202	-0.17549	0.10283	-1.2300	0.32895	0.88500	-0.37025
	0.56548	0.30106	0.76024	0.39114	0.30249	0.34080	0.64362	0.30636	0.66529	0.45518
	_____0.528_____		_____0.611_____				_____0.595_____			
	_____1.790_____		_____1.644_____				_____1.674_____			
Fe–H	-1.0935	0.26587			-0.40748	0.21988				
	0.77628	0.28633			0.45450	0.47301				
	0.8	0.8			0.8	0.8				
	2	2			2	2				
			B_1	p_1	B_2	p_2	r_1	r_c		
	Fe–C	771.190	2.3962	19.325	1.5555	0.50071	1.5070			
	Fe–H	299.563	2.69225			0.75	0.95			

that C–C interactions should not extend beyond the first neighbor distance in diamond,²⁸ as it is known that longer range terms do not improve tight binding models for diamond structure sp -bonded elements.^{29,30}

B. The C–C parameterization

Taking the view that carbon–carbon interactions are to be curtailed beyond the usual definition of the chemical bond lengths of 1.2–1.5 Å, none of the tests that we will apply in section III will require us to specify the C–C bond integrals or pair potential. There is however one notable exception which we will be discussing in greater detail below. This is the

observation from LSDA-GGA calculations¹⁰ that two carbon atoms bound to a monovacancy in Fe will form a “dimer molecule” whose bond length is 1.44 Å. In our model we have the freedom to choose our C–C interactions at will since they do not affect any of the results in the concentrated limit. It would be desirable if an existing model for diamond could be adopted without modification and we have used a tight binding Hamiltonian for diamond from Harrison²⁹ with parameters adapted by Xu *et al.*²⁸ (Our model is essentially that of Harrison in terms of the scaling of the bond integrals and pair potential with bond length. We take over the bond integrals at the equilibrium volume in diamond from Xu *et al.* but we do not adopt their scaling.) In this way for the C–C parameters we use a simple power law model, namely

$$h(r) = h_0 r^{-2} \quad , \quad \phi(r) = B_1 r^{-4}$$

with (in Rydberg a.u.)

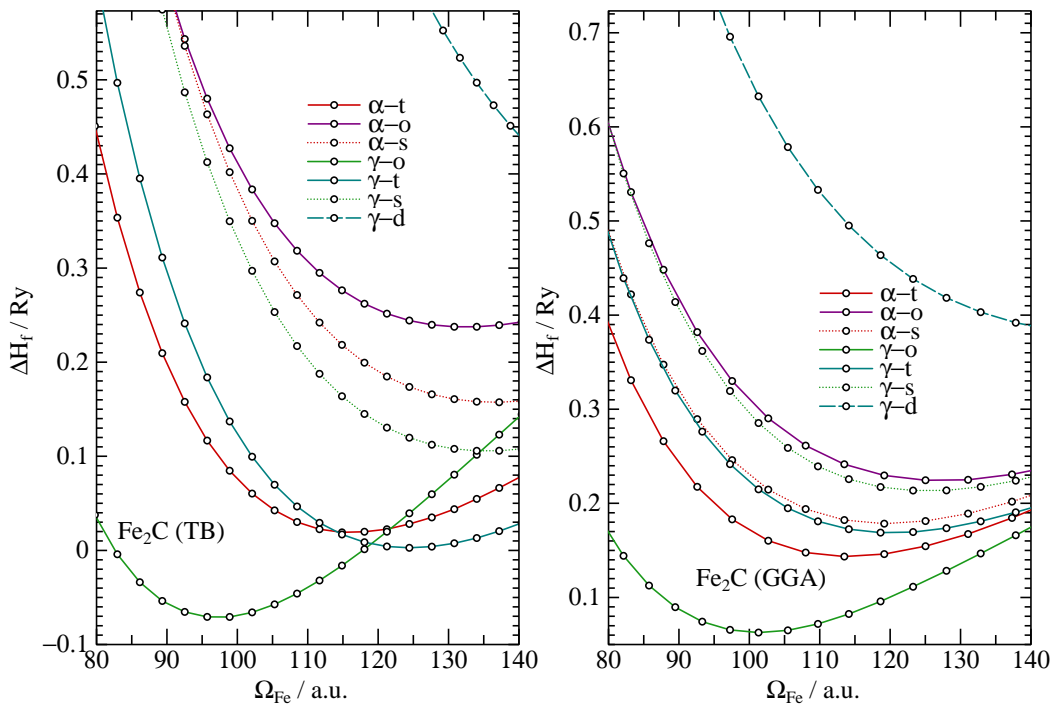
$$h_0^{ss\sigma} = -3.734 \quad h_0^{sp\sigma} = 3.510 \quad h_0^{pp\sigma} = 4.107 \quad h_0^{pp\pi} = -1.157$$

$B_1 = 50$ a.u. leads to the correct lattice constant *and* bulk modulus in diamond carbon. Unfortunately that choice of B_1 does not quite reproduce the energy and C–C bond length of the C_2 molecule bound to the Fe monovacancy. Therefore we employ $B_1 = 43$ a.u. which leads to about an 8% error in the diamond lattice constant. We have used the same value of B_1 to calculate the total energy of diamond which is the quantity we have used in figures 1–4 to determine the heat of formation of Fe–C compounds from elemental α -Fe and diamond C. This has the consequence that the tight binding theory consistently overestimates $-\Delta H_f$ by 0.16 Ry (see for example figure 1); if we use the value $B_1 = 50$ a.u. the agreement with the LSDA-GGA is rather better. To keep the C–C interactions to within the first neighbors as expected in diamond and in hydrocarbons, we apply a fixed multiplicative cut-off at $r_1 = 0.6a_0^{\text{bcc}}$ and $r_c = a_0^{\text{bcc}}$.

III. PREDICTIONS OF THE NEW MODEL

In this section we examine to what extent our model reproduces some previously published or our calculated LSDA-GGA data.

FIG. 2. (color online) Energy volume curves for compounds with stoichiometry Fe_2C , comparing the predictions of our model with results of our LSDA-GGA calculations. These compounds have either bcc (α) or fcc (γ) iron lattices with C placed at interstitial positions in tetrahedral (t), octahedral (o), in the bcc case the saddle point (s) along the $\langle 110 \rangle$ direction and, in the fcc case, the saddle points (s) along the $\langle 111 \rangle$ direction and (d) along the $\langle 110 \rangle$ direction. This latter site is midway between two nearest neighbor Fe atoms and so is expected to have a high energy; on the other hand as is known from LSDA-GGA calculations²⁷ and as our model also predicts, this site is along the diffusion path in γ -Fe. The alternative path for diffusion (adopted by H) *via* an intermediate tetrahedral site has higher energy. This is discussed in section III B.



A. The concentrated limit

We first compare tight binding with LSDA-GGA for a range of mostly fictitious Fe-C compounds with stoichiometries Fe_2C , Fe_3C , and Fe_4C in figures 2–4. The LSDA-GGA calculations were done by means of the mixed-basis pseudopotential (MBPP) method.^{31,32} The PBE-GGA exchange and correlation functional,³ optimally smooth norm conserving pseudopotentials³³ for Fe and C, \mathbf{k} -points which are equivalent to $8 \times 8 \times 8$ Chadi-Cohen meshes for cubic structures, and a Gaussian broadening by 0.2 eV were employed. The mixed

FIG. 3. (color online) Energy volume curves for compounds with stoichiometry Fe_3C , comparing the predictions of our model with results of our LSDA-GGA calculations. Here we show both interstitial, and substitutional putative phases all of which have large positive heats of formation and are hence predicted not to exist. The first four in the column of labels represent bcc and fcc supercells containing one vacancy and a C atom at either a neighboring tetrahedral (t) or octahedral (o) site. The next four are substitutional phases labeled using their *Strukturbericht* designations. Of greatest interest are the remaining three Fe_3C compounds: “WC” labels a hypothetical high energy structure similar to a simple hexagonal tungsten carbide like phase (see the text); the only phases predicted to exist thermodynamically are the ϵ carbide and the θ carbide, or cementite phase. It is interesting to note that the LSDA-GGA predicts these both to have a *positive* heat of formation, which requires further investigation, since they are both known to exist ubiquitously in the microstructures of steels.

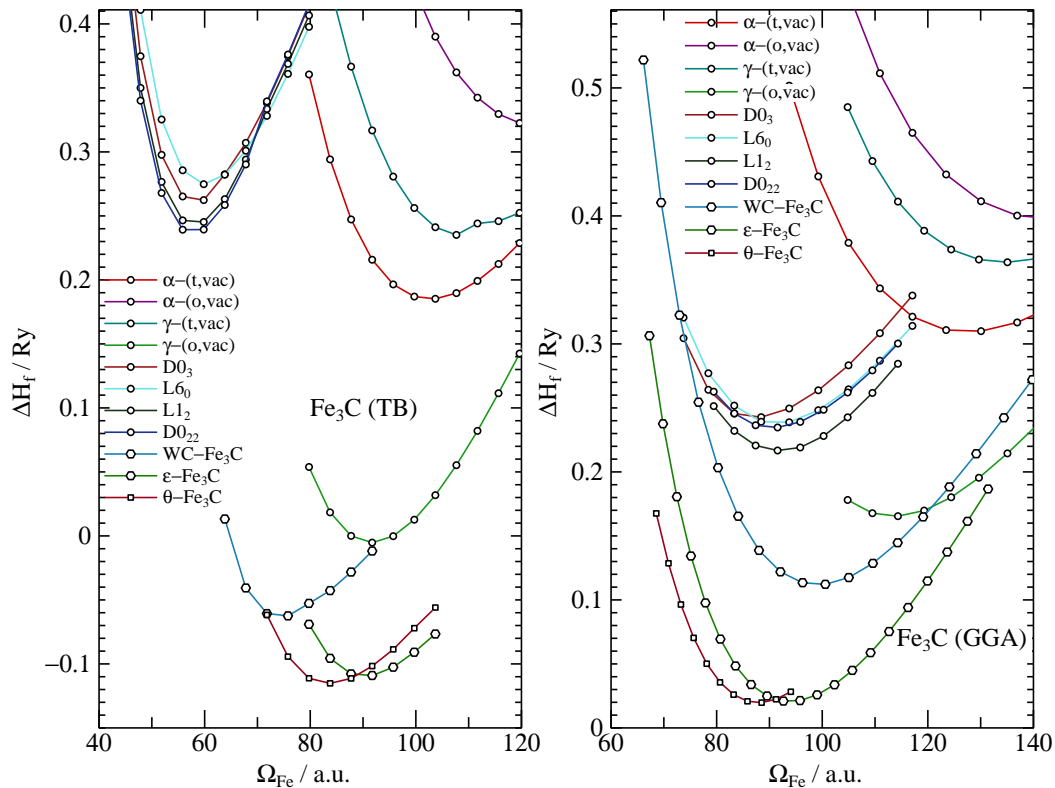
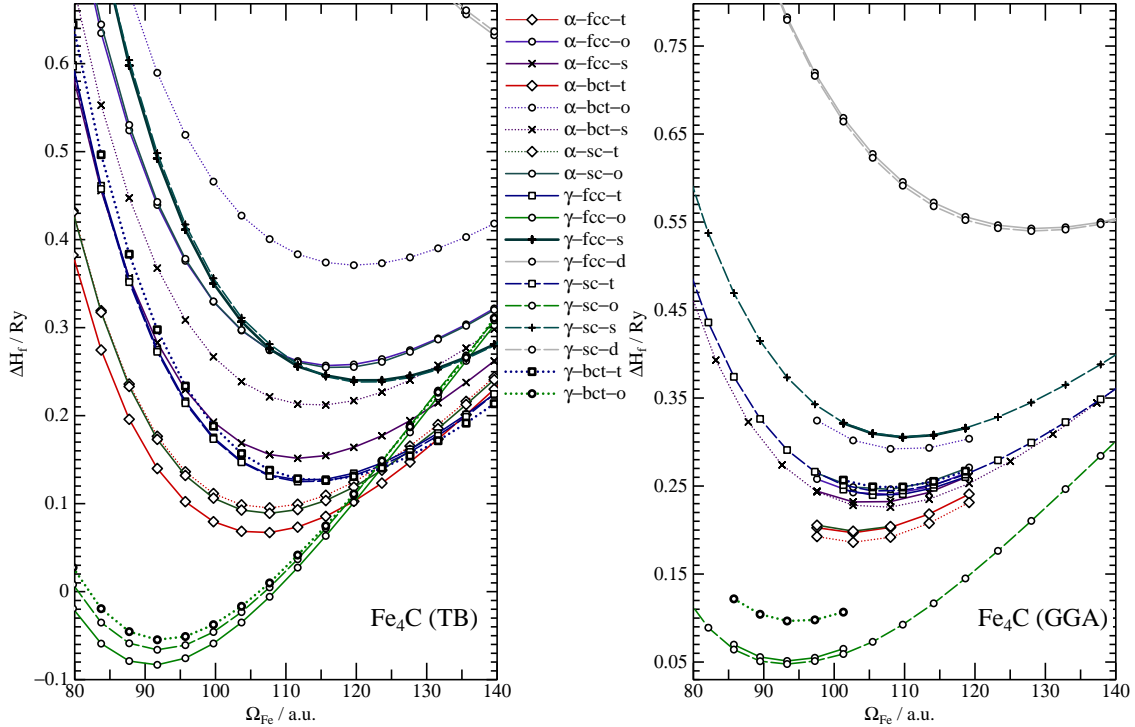


FIG. 4. (color online) Energy volume curves for compounds with stoichiometry Fe_4C , comparing the predictions of our tight binding model with our LSDA-GGA calculations. Here we show a variety of supercells in bcc (α) and fcc (γ) crystal structures, each in face centered cubic (fcc), body centered tetragonal (bct) and simple cubic (sc) supercell settings. In each of these cases, a C atom is placed at one of the interstitial sites, using the same labeling as in figure 2. As expected from the results of figure 1 and seen also in the data in figure 2 only the γ -Fe with octahedral carbon have reasonably low heats of formation.



basis consisted of plane waves up to a maximum kinetic energy of 340 eV and atom-centered basis functions with d -symmetry for Fe atoms and with p -symmetry for C atoms which are confined to spheres with radii of 1.19\AA and 0.66\AA respectively. The broad agreement between tight binding and LSDA-GGA is excellent and indeed in almost all instances the ordering in energy of the phases is correctly reproduced.

We will focus most closely on the stoichiometry Fe_3C , figure 3, which is the most significant composition in materials science due to the ubiquitous occurrence of cementite in the microstructures of steels. It is also notable that a significant weakness in the tight binding model emerges here when trying to describe the hypothetical *substitutional* phases D0_3 , L6_0 ,

TABLE VI. Calculated lattice parameters of hexagonal ϵ Fe₃C and orthorhombic θ Fe₃C (cementite), compared to LSDA-GGA calculations and experimental measurements reported by Jang *et al.*^{34,35} Lattice parameters a , b and c are in Å. The last column shows the predicted equilibrium volume compared to experiment.

		a	b	c	b/a	c/a	V/V_{exp}
θ -Fe ₃ C	TB	4.95	6.79	4.42	1.37	0.89	0.96
	LSDA-GGA	5.13	6.65	4.46	1.30	0.86	0.98
	exp.	5.09	6.74	4.52	1.32	0.89	
ϵ -Fe ₃ C	TB	4.63		8.64		1.87	0.93
	LSDA-GGA	4.74		8.63		1.82	0.98
	exp.	4.77		8.71		1.83	

L1₂, and D0₂₂. This is not so surprising since this bonding environment is very different from the *interstitial* phases and fortunately the substitutional phases are not of particularly great interest. It is on the other hand very gratifying that the tight binding model reproduces with great fidelity the ϵ and θ iron carbide phases. At the same time the ordering of the unfavorable simple hexagonal tungsten carbide like structure is very well rendered; this hypothetical structure is obtained from the hexagonal close packed ϵ -Fe₃C by rotating alternate Fe layers about the c -axis by 60° and increasing the axial ratio by $\sqrt{3/2}$. To emphasise the suitability of the tight binding approximation in the modeling of steel microstructures, we show in table VI a detailed comparison of the calculated crystal lattice parameters of the important phases, ϵ and θ iron carbide, with experimental data.

B. The dilute limit

Of equal or even greater interest is the behavior of carbon in the dilute limit. In the case of hydrogen in Fe we could claim a success in that a model fitted in the most concentrated stoichiometry transfers very well into the dilute limit.¹⁷ Carbon in Fe has been more problematic and subsequent to the fitting described in section II A it was necessary to make further genetic optimizations of the Fe–C parameters in order to render correctly the migration energy and the binding of C to a monovacancy—the quantities $H_C^{\text{M}\alpha}$ and $E_B(1)$ in the first two data columns of table VII.

TABLE VII. Properties of C in Fe in the dilute limit. $H_C^{M\alpha}$ is the migration energy of the C atom, equal to the energy difference between C in tetrahedral and octahedral interstices in bcc α -Fe. $E_B(1)$ and $E_B(2k)$ are the binding energies of one and two C atoms to a vacancy (see ref [11], table 5). The final two columns are data for C in fcc γ -Fe and show the migration energies $H_C^{M\gamma}(\text{tet})$ and $H_C^{M\gamma}(\text{d})$ of C between two octahedral sites *via* a tetrahedral site and the “d-saddle” site respectively. All energies are in eV. The first line shows LSDA-GGA data taken from refs [9], [27] and [14]. The second line shows results from our TB model.

	$H_C^{M\alpha}$	$E_B(1)$	$E_B(2k)$	$H_C^{M\gamma}(\text{tet})$	$H_C^{M\gamma}(\text{d})$
LSDA-GGA	0.87	0.47	1.50	1.48	1.00
TB	0.81	0.35	1.55	2.11	0.63

TABLE VIII. Comparative energies and bond lengths of four possible configurations of two carbon atoms bound to one vacancy in bcc α -Fe. We use the designations of refs [9] and [14]. The structures relaxed using TB are illustrated in figure 5. The first and second rows show results from LSDA-GGA calculations and the third and fourth those from the TB model. The latter correctly predicts the ordering in energy (these are shown relative to the “k” ground state energy) and the bond length. The “ $\langle 110 \rangle$ ” configuration has the dimer centered at the vacant Fe site and orientated along a $\langle 110 \rangle$ direction. Energy differences ΔE are in eV and bond lengths d in Å. The numbers in parentheses are energy differences calculated using the Fe atom positions of the relaxed equivalent structure, with both C atoms removed; these numbers allow a comparison of the host lattice distortions accompanying the formation of the dimer–vacancy complex.

	“j”		“ $\langle 100 \rangle$ ”		“k”		“ $\langle 110 \rangle$ ”	
	ΔE	d	ΔE	d	ΔE	d	ΔE	d
LSDA-GGA	0.37	2.57	0.11	1.46	0	1.43	0.06	1.43
	(0.07)		(−0.05)		(0)		(0.04)	
TB	1.10	2.70	0.13	1.46	0	1.44	1.23	1.40
	(0.49)		(0.16)		(0)		(0.66)	

Our main results are presented in tables VII and VIII. We have constructed cubic $4 \times 4 \times 4$ supercells for α -Fe and γ -Fe in order to study, in particular, the energetics of the monovacancy in Fe and its binding to carbon interstitials. As in the case of hydrogen, the impurity does not occupy a vacant Fe lattice site, as is clear from figure 3 which shows a large positive heat of formation for the four substitutional phases considered. Instead (again, as does hydrogen) carbon occupies a position close to its preferred interstitial site, in this case the octahedral interstice, at one of the cube faces bounding the vacancy. We follow the definitions employed by Becquart *et al.*¹¹ such that the binding energy of one or more interstitials to a vacancy is the difference in energy between that number of interstitials and the vacancy occupying separate, non interacting sites, and the interstitials bound to the vacancy. In this way, we have, from calculations based on a 128-atom supercell of pure Fe,

$$E_B(1) = -(E(\text{Fe}_{127}\text{C}) + E(\text{Fe}_{128})) + (E(\text{Fe}_{127}) + E(\text{Fe}_{128}\text{C}))$$

and

$$E_B(2) = -(E(\text{Fe}_{127}\text{C}_2) + 2E(\text{Fe}_{128})) + (E(\text{Fe}_{127}) + 2E(\text{Fe}_{128}\text{C}))$$

where the signs are employed such that a positive binding energy implies a preference for the two C atoms to bind at a vacancy compared to the vacancy and two C interstitials being widely separated. The total energies E involved are calculated by relaxing supercells containing the numbers of atoms indicated in parentheses.

We therefore show in table VII $E_B(1)$, the binding energy of a single C atom to a monovacancy, and $E_B(2k)$ (using the designations of Becquart *et al.*¹¹) the binding energy of two C atoms to a vacancy.

We have also calculated migration energies of carbon in α -Fe and γ -Fe using static relaxations and also the nudged elastic band method.³⁶ TB describes these correctly in both phases of Fe as seen in the data columns 1, 4, and 5 in table VII. In particular our TB model confirms the LSDA-GGA result that the diffusion path of C in γ -Fe is *not* as one might suppose mediated by a “double” hop *via* a neighboring tetrahedral site as for H in γ -Fe, but the carbon atom actually takes a direct route forcing itself through the bond center of two nearest neighbor Fe atoms at the $\langle 110 \rangle$ (d) saddle point. This is surprising in view of the high energy of the γ -d crystal structures in figures 3 and 4. However this tight binding prediction agrees with LSDA-GGA results.³⁷

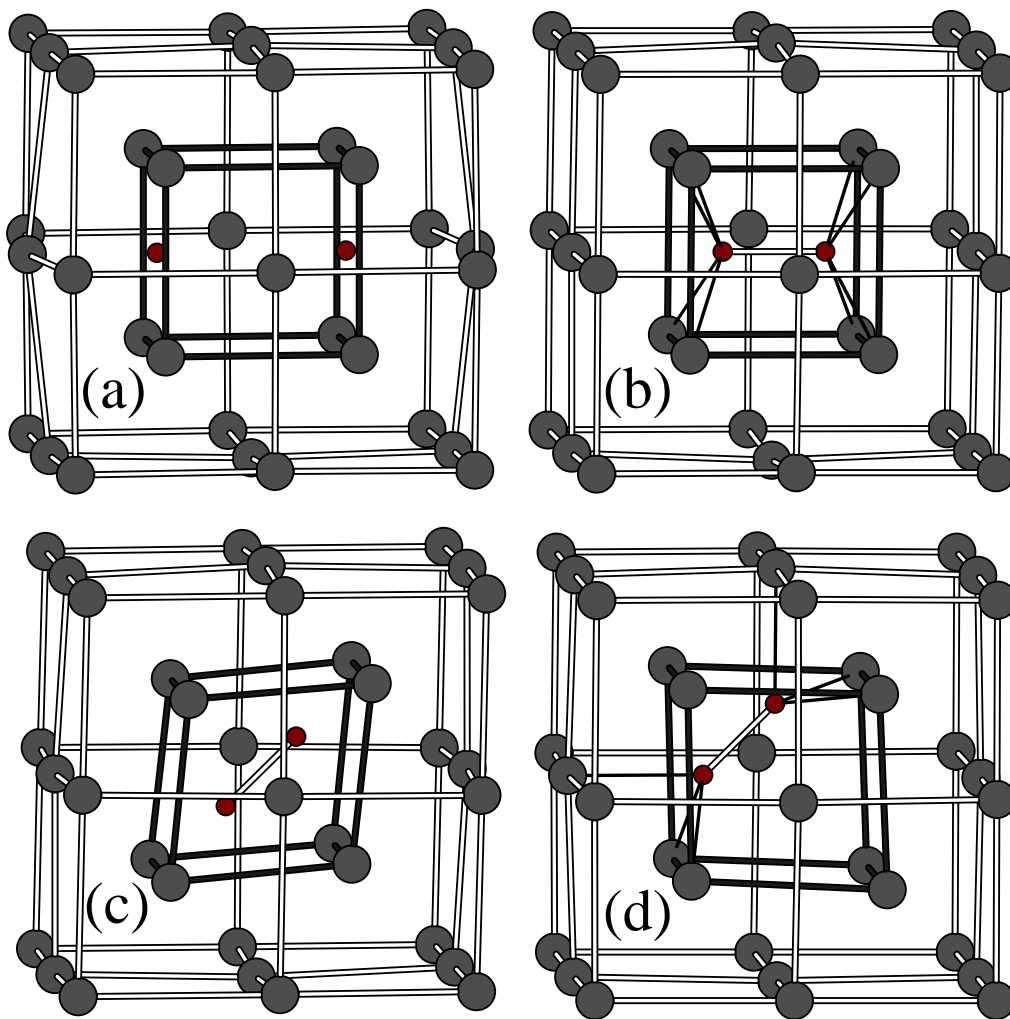
C. The carbon dimer at the vacancy

Several authors have made LSDA-GGA calculations for a carbon dimer bound to a vacancy in α -Fe and described a number of possible atomic structures.^{10,11,14} We consider four here. If the dimer is orientated along a $\langle 100 \rangle$ direction, then if the carbon atoms remain close to their original octahedral sites at opposite faces of the cube bounding the vacancy, this configuration is designated “j” by Becquart *et al.*¹¹ or “OO” by Lau *et al.*¹⁴ This is a *local minimum* in the energy and in our TB model the two carbon atoms are outside their range of interaction in the Hamiltonian (see section II B). The energy is lowered if the two carbon atoms approach each other along the $\langle 100 \rangle$ direction and form a dimer bond, having a bond length of 1.46Å which is very close to that in diamond and the C–C single bond in molecules. This configuration is denoted “ $\langle 100 \rangle$ ” by Lau *et al.*¹⁴ but was not considered in earlier work.^{10,11} This is not yet the global minimum energy for the dimer which is achieved by orientating the dimer along a $\langle 011 \rangle$ direction with the two C atoms close to octahedral positions, a situation denoted “k” by Becquart *et al.*¹¹ or “AO” by Lau *et al.*¹⁴ The latter authors describe a further configuration, “ $\langle 011 \rangle$ ” in which the dimer bond is centered at the vacant site and orientated parallel to “k”. This is of slightly higher energy than “k”. The four configurations are illustrated in figure 5. In table VIII we compare predictions of the TB model with our own LSDA-GGA results.³⁸ The only serious discrepancy is that the TB model overestimates the energies of the “j” and “ $\langle 011 \rangle$ ” configurations with respect to LSDA-GGA.

IV. DISCUSSION

Först *et al.*¹ made a very thorough study using LSDA-GGA of point defect complex energetics and found the remarkable result that under the conditions normally encountered in a steel, effectively *all Fe vacancies have a C₂ dimer bound to them* as illustrated in figure 5. Moreover, by just a few hundredths of an eV, the dimer prefers to be orientated along a $\langle 110 \rangle$ direction. It would be of great interest to determine whether this phenomenon can be confirmed experimentally, possibly by internal friction measurements. It is notable that a similar prediction was made using DFT concerning dimerization of boron in copper, a prediction that is consistent with thermodynamic assessment.⁴¹

FIG. 5. (color online) Atomic structures of four configurations for a carbon dimer bound to a mono-vacancy in α -Fe. Structures shown are (a) “j” [11], or “OO” [14]; (b) “ $\langle 100 \rangle$ ” [14]; (c) “ $\langle 110 \rangle$ ” [14]; (d) “k” [11] or “AO” [14], the global minimum for this configuration.¹⁴ The relaxed structures displayed here are obtained with our TB model; Fe–C bond lengths shown are 3.73Å in “ $\langle 100 \rangle$ ” and 3.65Å in “k”



One can interpret the competition between the four configurations illustrated in figure 5 in terms of certain notional contributions to the total energy. These are (i) the formation of a C–C covalent bond, (ii) the coordination of the carbon atoms to neighboring Fe atoms, and (iii) the accompanying distortion of the host Fe lattice containing a vacancy. (i) It is surprising that a C–C bond having the same length as in pure carbon is formed in view of the metallic electron gas destroying the single bond order; the bond length inside the metal is the same as in the pure carbon or hydrocarbon, but the bond energy is about ten times smaller. (ii) The Fe–C coordination goes a long way to explain the stability of the most stable configuration “k” in which the carbon dimer makes three bonds of equal length (3.65Å) to Fe atoms, thus forming an “ethane” molecule in which the Fe atoms take the part of H atoms (see figure 5(d)). With the dimer orientated along $\langle 100 \rangle$ each carbon atom makes four bonds (3.73Å long) to neighboring Fe atoms (figure 5(b)). We take it that this is less favorable owing to carbon preferring a four fold coordination. Configurations “j” and “ $\langle 110 \rangle$ ” both display a planar configuration of Fe–C bonds; in “j” the carbon is bonded to four Fe atoms in the plane of a cube face of the bcc lattice, in “ $\langle 110 \rangle$ ” each carbon is bonded to two Fe atoms. (iii) In table VIII we give in parentheses values of the calculated total energies of the four configurations, *having removed the two carbon atoms* and leaving the Fe atoms in their positions. This is intended to examine the elastic distortion energy accompanying the introduction of the dimer into the vacancy. In the LSDA-GGA these distortion energies are rather small and in fact “ $\langle 100 \rangle$ ” has a slightly lower value than “k”. However the preferred four fold coordination of the carbon atoms in “k” is able to compensate for the increased distortion energy. Whereas the TB model correctly predicts “k” to be the global minimum, the quantitative comparison with LSDA-GGA is rather poor. We suppose that this is a consequence of the small basis set of TB and more limited self consistency. Thus TB *overestimates* effects based on covalent bonding and lattice distortions because the Hamiltonian does not have the degrees of freedom of LSDA-GGA to find a lower energy in the case of an unfavorable structure. This is well illustrated in the case of “ $\langle 110 \rangle$ ” in figure 5(c). Clearly there is a large distortion of the bcc cubic unit cell surrounding the vacancy. The LSDA-GGA given the constraint of this distortion in the *atomic* structure is yet able to find a low energy *electronic* structure that can accommodate the constraint. The TB finds this much more difficult.

V. CONCLUSIONS

The TB model presented here is intended as a physically better motivated and more transferable scheme as compared to the recently published orthogonal pd -model¹⁵ or to existing classical interatomic potentials. Its transferability has been demonstrated using tests in both concentrated and dilute limits, for example successfully predicting the structure and energetics of cementite (section III A) and the migration path of C in γ -Fe (section III B). It may be thought that this migration path particularly would expose the need for environment dependence in an empirical model^{42,43} Our model, using only two-center parameters, is able to deal with this through the use of an overlap matrix between non orthogonal Fe and C orbitals.^{20,44}

Our model also correctly describes the structure and energetics of the carbon dimer bound to a vacancy in α -Fe—a defect that is expected to take a central importance following the predictions of Först *et al.*¹ Apart from a large overestimation of the energy of the “ $\langle 011 \rangle$ ” dimer, our TB model properly orders the structures and predicts “k” to have the lowest energy although we were forced to modify an existing simple model for carbon in order to achieve the correct C₂ bond length (see section II B). It is notable that published classical potentials¹¹ and the minimal basis TB model¹⁵ cannot reproduce the stability of the carbon dimer. An exception is the recent classical potential of Lau *et al.*¹⁴ although this model greatly *overestimates* the binding energy of the $\langle 011 \rangle$ dimer.

In view of the apparent significance of carbon dimers existing in the microstructure of steel and their possible interactions with hydrogen¹² it is now a matter of importance that plausible and efficient quantum mechanical models are produced. From this point of view the present work assumes a particular significance.

ACKNOWLEDGMENTS

It is a pleasure to thank Charlotte Bequart for a helpful correspondence. This work was undertaken as a part of the project MultiHy of the European Union’s 7th Framework Programme (MultiHy.eu). Financial support from the German Federal Ministry for Education and Research (BMBF) to the Fraunhofer IWM for C. E. (Grant number 02NUK009C) is

gratefully acknowledged.

-
- * Present address: National Physical Laboratory, Teddington, Middlesex, TW11 0LW, UK
and Department of Physics, King's College London, Strand, London WC2R 2LS, UK;
Tony.Paxton@KCL.ac.uk
- † Christian.Elsaesser@iwm.fraunhofer.de
- ¹ C. J. Först, J. Slycke, K. J. Van Vliet, and S. Yip, Phys. Rev. Lett. **96**, 175501 (2006).
- ² D. G. Pettifor, *Bonding and structure of molecules and solids* (Oxford University Press, Oxford, 1995).
- ³ J. P. Perdew, K. Burke, and M. Ernzerhof, Phys. Rev. Lett. **78**, 1396 (1997).
- ⁴ U. K. Poulsen, J. Kollár, and O. K. Andersen, J. Phys. F: Metal Phys. **9**, L241 (1976).
- ⁵ N. E. Christensen, O. Gunnarsson, O. Jepsen, and O. K. Andersen, J. de Phys. Colloque C8 **49**, 17 (1988).
- ⁶ G. Liu, D. Nguyen-Manh, B.-G. Liu, and D. G. Pettifor, Phys. Rev. B **71**, 174115 (2005).
- ⁷ A. T. Paxton and M. W. Finnis, Phys. Rev. B **77**, 024428 (2008).
- ⁸ S. L. Dudarev and P. M. Derlet, J. Phys.: Condens. Matter. **17**, 7097 (2005).
- ⁹ C. Domain and C. S. Becquart, Phys. Rev. B **65**, 024103 (2001).
- ¹⁰ C. Domain, C. S. Becquart, and J. Foct, Phys. Rev. B **69**, 144112 (2004).
- ¹¹ C. Becquart, J. Raulot, G. Bencteux, C. Domain, M. Perez, S. Garruchet, and H. Nguyen, Computational Materials Science **40**, 119 (2007).
- ¹² P. R. Monasterio, T. T. Lau, S. Yip, and K. J. Van Vliet, Phys. Rev. Lett. **103**, 085501 (2009).
- ¹³ M. Kabir, T. T. Lau, X. Lin, S. Yip, and K. J. Van Vliet, Phys. Rev. B **82**, 134112 (2010).
- ¹⁴ T. T. Lau, C. J. Först, X. Lin, J. D. Gale, S. Yip, and K. J. Van Vliet, Phys. Rev. Lett. **98**, 215501 (2007).
- ¹⁵ N. Hatcher, G. K. Madsen, and R. Drautz, Phys. Rev. B **86**, 155115 (2012).
- ¹⁶ R. Drautz and D. G. Pettifor, Phys. Rev. B **84**, 214114 (2011).
- ¹⁷ A. T. Paxton and C. Elsaesser, Phys. Rev. B **82**, 235125 (2010).
- ¹⁸ M. W. Finnis, A. T. Paxton, M. Methfessel, and M. van Schilfgaarde, Phys. Rev. Lett. **81**, 5149 (1998).
- ¹⁹ G. K. H. Madsen, E. J. McEniry, and R. Drautz, Phys. Rev. B **83**, 184119 (2011).

- ²⁰ A. Urban, M. Reese, M. Mrovec, C. Elsässer, and B. Meyer, *Phys. Rev. B* **84**, 155119 (2011).
- ²¹ H.-P. Schwefel, *Evolution and Optimum Seeking: The Sixth Generation* (John Wiley, New York, 1993).
- ²² D. G. Pettifor, *Journal of Physics F: Metal Physics* **7**, 613 (1977).
- ²³ O. K. Andersen, O. Jepsen, and D. Glötzel, “Highlights of condensed matter theory,” (North-Holland, New York, 1985) Chap. 3.
- ²⁴ A. T. Paxton, *Journal of Physics D: Applied Physics* **29**, 1689 (1996).
- ²⁵ A. Seeger, *phys. stat. sol. (a)* **167**, 289 (1998).
- ²⁶ D. Pashov, *Electronic structure of certain Titanium-Aluminium superalloys: from first principles to Bond Order Potentials*, Ph.D. thesis, Queen’s University Belfast (2012).
- ²⁷ D. E. Jiang and E. A. Carter, *Phys. Rev. B* **67**, 214103 (2003).
- ²⁸ C. H. Xu, C. Z. Wang, C. T. Chan, and K. M. Ho, *Journal of Physics: Condensed Matter* **4**, 6047 (1992).
- ²⁹ W. A. Harrison, *Electronic structure and the properties of solids* (W. H. Freeman, San Francisco, 1980).
- ³⁰ A. T. Paxton, A. P. Sutton, and C. M. M. Nex, *Journal of Physics C: Solid State Physics* **20**, L263 (1987).
- ³¹ C. Elsässer, N. Takeuchi, K. M. Ho, C. T. Chan, P. Braun, and M. Fähnle, *Journal of Physics: Condensed Matter* **2**, 4371 (1990).
- ³² F. Lechermann, F. Welsch, C. Elsässer, C. Ederer, M. Fähnle, J. M. Sanchez, and B. Meyer, *Phys. Rev. B* **65**, 132104 (2002).
- ³³ D. Vanderbilt, *Phys. Rev. B* **32**, 8412 (1985).
- ³⁴ J. H. Jang, I. G. Kim, and H. K. D. H. Bhadeshia, *Computational Materials Science* **44**, 1319 (2009).
- ³⁵ J. H. Jang, I. G. Kim, and H. K. D. H. Bhadeshia, *Scripta Materialia* **63**, 121 (2010).
- ³⁶ G. Henkelman and H. Jonsson, *J. Chem. Phys.* **113**, 9978 (2000).
- ³⁷ D. E. Jiang and E. A. Carter, *Phys. Rev. B* **70**, 064102 (2004).
- ³⁸ For these LSDA-GGA calculations, in order to get the best comparison with refs [9], [11] and [14] we used the VASP code^{39,40} (version 4.6) with ultrasoft pseudopotentials and a plane wave basis (energy cut off 500eV) instead of the MBPP code. All other computational settings are as in section III A. We made sure that the MBPP and VASP results for the four C₂ configurations

agreed very closely for cubic $3 \times 3 \times 3$ supercells and then treated $4 \times 4 \times 4$ supercells only with VASP.

- ³⁹ G. Kresse and J. Furthmüller, *Computational Materials Science* **6**, 15 (1996).
- ⁴⁰ G. Kresse and D. Joubert, *Phys. Rev. B* **59**, 1758 (1999).
- ⁴¹ A. Y. Lozovoi and A. T. Paxton, *Phys. Rev. B* **77**, 165413 (2008).
- ⁴² M. S. Tang, C. Z. Wang, C. T. Chan, and K. M. Ho, *Phys. Rev. B* **53**, 979 (1996).
- ⁴³ H. Haas, C. Z. Wang, M. Fähnle, C. Elsässer, and K. M. Ho, *Phys. Rev. B* **57**, 1461 (1998).
- ⁴⁴ D. Nguyen-Manh, D. G. Pettifor, and V. Vitek, *Phys. Rev. Lett.* **85**, 4136 (2000).